The Unusual Fluxional Structure of Tetramethyloxotungsten: Quantum Chemical Structure Predictions for the d^0 and d^1 Complexes [MOR$_4$] (M = W, Re; R = H, CH$_3$)**

Martin Kaupp*

Dedicated to Professor Dr. Hans-Georg von Schnering

Abstract: An unprecedented, highly fluxional structure is predicted for the d^0 complex tetramethyloxotungsten, [WO(CH$_3$)$_4$] (**2**), from density functional and ab initio calculations: The lowest energy structure **2C$_s$-1** on the potential energy surface may be described equally well as a distorted trigonal bipyramidal or distorted square pyramidal arrangement. Four equivalent minima **2C$_s$-1** may interconvert rapidly via four equivalent, low-lying transition states **2C$_s$-2** (ca. 3 kJ mol^{-1} above **2C$_s$-1**). The more conventional regular square pyramidal structure **2C$_{4v}$-1** is found to have a twofold degenerate imaginary vibrational mode. It thus also serves as a transition state (only ca. 8 kJ mol^{-1} above **2C$_s$-1**). Interestingly, rotation of the methyl groups is severely hindered in this square pyramidal structure, whereas it is easy for some of the methyl groups in the distorted structures. Thus, the methyl group conformations and the skeletal distortions appear to be strongly coupled due to agostic interactions. Comparisons are made with the model d^0 oxohydride [WOH$_4$] (**1**), and to the corresponding d^1 complex [ReOH$_4$] (**3**), which are also fluxional but differ from **2** and from each other. The related d^1 complex [ReO(CH$_3$)$_4$] (**4**) prefers the experimentally confirmed conventional square pyramidal structure **4C$_{4v}$-1**, but is found also to have unusually high barriers for methyl group rotation. Computed IR spectra might aid the experimental structure analysis for tetramethyloxotungsten. Somewhat surprisingly, the predicted ^{17}O NMR chemical shifts may also provide an indirect test for the structural distortions. The electronic structure characteristics and the competition between σ- and π-bonding in these interesting compounds are discussed, and are related to other d^0 and d^1 species by natural population analysis and frontier orbital arguments. Further low-symmetry structures are suggested.

Keywords: agostic interactions · density functional calculations · fluxionality · rhenium · tungsten

Introduction

Early transition metal complexes with a formal d^0 electronic configuration at the metal may, under certain circumstances, adopt less symmetrical structures than those predicted by the usual structural models. In the past, most theoretical and experimental work has concentrated on the simplest homoleptic complexes. Examples range from bent instead of linear two-coordinate[1–4] via pyramidal rather than planar three-coordinate[5] to regular or distorted trigonal prismatic instead of octahedral six-coordinate[6–12] complexes. Of the factors controlling the structures of such complexes, optimal involvement of the metal d orbitals in σ-bonding to the ligands and the polarization of the outermost metal core shell lead to a preference for the low-symmetry arrangements. Repulsions between the ligands and π-bonding favor the classical high-symmetry structures.

In the case of pentacoordination, it is well known that the trigonal bipyramidal and the square pyramidal structures tend to be close in energy.[13–15] In main-group chemistry, the trigonal bipyramid is considered to be favored slightly owing to lower ligand repulsion (assuming no lone pairs have to be accommodated). In the case of d^0 complexes, the operation of the above-mentioned electronic factors has been confirmed during the last few years. Thus, purely σ-bound ligands tend to favor the square pyramid. This has been found experimentally for [Ta(CH$_3$)$_5$][16] and for [Ta{CH$_2$(4-MeC$_6$H$_4$)}$_5$],[17] and computationally for [TaR$_5$ (R = H, CH$_3$)].[7, 18] π-Donor ligands reverse this tendency and lead to a preference for a trigonal bipyramid, for example for d^0 pentahalides (however, the energy differences may be quite small; see examples given in ref. [7]).

[*] Priv.-Doz. Dr. M. Kaupp
    Max-Planck-Institut für Festkörperforschung
    Heisenbergstrasse 1, D-70569 Stuttgart (Germany)
    E-mail: kaupp@vsibm1.mpi-stuttgart.mpg.de

For mixed-ligand systems, an interesting competition between π- and σ-bonding preferences may be expected. In this work, we use density functional and ab initio calculations to address the question of which structures are preferred for MXR_4 systems with one π-donor ligand X and four pure σ-donors R. We will focus on the organometallic oxo complex tetramethyloxowtungsten, $[WO(CH_3)_4]$, and on the related d^0 system $[WOH_4]$ and d^1 species $[ReOR_4]$ (R = H, CH_3). The related halogeno complexes $[MOHal_4]$ (M = Mo, W, Re) have regular, unremarkable square pyramidal structures in the gas phase, with the oxo ligand in apical position.[19] This classical ligand arrangement provides a suitable reference point with which the present, more unusual systems contrast markedly. Tetramethyloxowtungsten was chosen as it might also be accessible experimentally. Our quantum chemical structure predictions, augmented by detailed IR and NMR spectroscopic calculations, should aid experimental studies on this and related systems, which have been initiated.[20] Beyond the specific compounds chosen, the theoretical study is also intended provide a more general framework to discuss the structures of such d^0 and d^1 $[MXR_4]$ systems. The d^1 rhenium complexes should give additional insight into the effect of adding one electron to the system.

Of the systems studied here, only $[ReO(CH_3)_4]$ is definitely known experimentally.[21, 22] It has been well characterized, both spectroscopically[21] and structurally (it exhibits a regular square pyramidal structure in the gas phase),[22] but has not yet been studied by first-principles quantum chemical calculations. It serves here mainly for comparison purposes, but also turns out to exhibit some interesting features in its own right. The hypothetical molecule $[MoOH_4]$, which is closely related to $[WOH_4]$ investigated here, has been studied previously by computations,[23, 24] for example as the simplest model system for some molybdenum enzymes. However, these calculations were restricted to a regular square pyramidal structure. The present results indicate that this arrangement is not a minimum on the potential energy surface.

After the present paper had been submitted, an interesting related article by Ward et al.[25] appeared, which studies the structures of d^0 MX_2R_3 systems, that is, complexes with two π-donor ligands (DFT and extended Hückel calculations on model systems were carried out, as well as structure correlation analyses). The present results will be compared with their study, as well as to other experimental and computational examples throughout the discussion.

Abstract in German: *Eine neuartige, hochgradig fluktuierende Struktur wird durch Dichtefunktional- und Ab-Initio-Rechnungen für Tetramethyloxowwolfram, $[WO(CH_3)_4]$ **(2)**, vorhergesagt: Die Struktur niedrigster Energie, $2C_s$-1, kann entweder als verzerrt trigonal prismatisch oder als verzerrt quadratisch-pyramidal beschrieben werden. Vier energetisch äquivalente Strukturen $2C_s$-1 können sich leicht über vier energetisch niedrig liegende (ca. 3 kJ mol^{-1} über $2C_s$-1), ebenfalls äquivalente Übergangszustände $2C_s$-2 ineinander umlagern. Für die konventionellere, regulär quadratisch-pyramidale Struktur $2C_{4v}$-1 wird eine zweifach entartete imaginäre Schwingungsmode gefunden. Diese Struktur entspricht daher ebenfalls einem Übergangszustand mit einer Energie, die um ca. 8 kJ mol^{-1} größer ist als die von $2C_s$-1. Interessanterweise ist die Rotation der Methylgruppen in der quadratisch-pyramidalen Struktur signifikant gehindert, während sie für einige der Methylgruppen in den verzerrten Strukturen leicht ist. Die Konformationen der Methylgruppen sind also aufgrund agostischer Wechselwirkungen stark an die Verzerrungen des Schweratomskelettes gekoppelt. Die Struktur **2** wird mit den d^0- und d^1-Modellverbindungen $[WOH_4]$ **(1)** bzw. $[ReOH_4]$ **(3)** verglichen, die ebenfalls fluktuierende Strukturen haben, sich aber charakteristisch von **2** und voneinander unterscheiden. Der verwandte d^1-Komplex $[ReO(CH_3)_4]$ **(4)** bevorzugt die experimentell bestätigte reguläre quadratisch-pyramidale Geometrie $4C_{4v}$-1, weist aber ebenfalls ungewöhnlich hohe Barrieren für die Rotation der Methylgruppen auf. Die berechneten IR-Spektren könnten zur Strukturanalyse für Tetramethyloxowwolfram beitragen. Überraschenderweise sollten die vorhergesagten ^{17}O-NMR-Verschiebungen ebenfalls zum indirekten Nachweis der verzerrten Strukturen nützlich sein. Die Charakteristika der Elektronenstruktur sowie die Konkurrenz zwischen σ- und π-Bindungen in diesen interessanten Verbindungen werden anhand von natürlichen Populationsanalysen und Grenzorbital-Argumenten diskutiert und mit denen anderer niedersymmetrischer d^0- und d^1-Verbindungen verglichen. Weitere Strukturen mit reduzierter Symmetrie werden vorgeschlagen.*

Computational Details

In our previous study of the d^0 complex $[W(CH_3)_6]$,[9] we found that the structure and energy characteristics computed using density functional theory (DFT) with gradient-corrected exchange-correlation functionals agree excellently with the results of more sophisticated post-Hartree–Fock treatments [MP2, CCSD, CCSD(T)]. Throughout a recent extended study of homoleptic d^0, d^1 and d^2 hexamethyl complexes,[12] and in the present work, we have thus concentrated on the more economical DFT methods (however, see below), using Becke's exchange functional[26] and Perdew's correlation functional[27] (this combination is frequently denoted as BP86). The basis sets correspond to basis A of ref. [9]. Thus, quasirelativistic effective core potentials (ECPs) with a small-core definition and 6s5p3d GTO valence basis sets[28] are used for the metals. Carbon and oxygen ECPs and DZP valence basis sets[29] are also as in refs. [9, 12]. In the case of MOH_4, the hydrogen DZ basis[30] was augmented by one set of p functions ($\alpha = 1.0$). All six cartesian components of the d functions were retained. We note in passing that the use of ab initio derived ECPs in DFT applications is well validated for the core sizes employed here.[9, 31] Unrestricted Kohn–Sham calculations were used for the open-shell (doublet d^1) systems $[ReOR_4]$.

Preliminary DFT optimizations without symmetry used the deMon program,[32] which allows a reduction of the computational effort by fitting the charge density and exchange-correlation potential with the help of auxiliary basis sets. Based on the results of these preliminary optimizations, the final calculations were carried out with the Gaussian 94 and Gaussian 92/DFT programs,[33] which do not employ charge-density or exchange-correlation potential fitting (the fine-grid option was generally used for numerical integrations). All structures have been fully optimized within a given point-group symmetry. The nonsymmetrical transition state $1C_1$-TS was optimized with quadratic synchronous transit (QST) algorithms.[34] All stationary points were characterized by harmonic vibrational frequency analyses (by means of numerical differentiation of analytical first energy derivatives). Natural population analyses[35] (NPA) used the built-in subroutines of the Gaussian program packages.[33]

CCSD(T) single-point energy calculations for [WOH$_4$] and [ReOH$_4$] with the MOLPRO program[36] used the DFT-optimized structures and added one metal f function[37] to the basis set. A UCCSD(T) approach[36b] was used for the rhenium complex. These calculations employed five-component d functions.

NMR chemical shifts were calculated within the SOS-DFPT approach[38, 39] with the IGLO choice of gauge origin[40] by the deMon-NMR program.[32, 38, 39] These calculations employed the optimized structures, the PW91 exchange-correlation potential,[41] and IGLO-II all-electron basis sets[40] for the ligand atoms (see ref. [9] for more details of the NMR chemical shift calculations). ^{13}C and ^{1}H shifts are given with respect to the absolute shieldings computed at the same level for tetramethylsilane, TMS (σ^{13}C = +187.5 ppm and σ^1H = +31.00 ppm), whereas ^{17}O shifts are given with respect to H$_2$O$_{liq}$ (σ^{17}O = 271 ppm, derived from the computed shielding of σ^{17}O = 307 ppm for H$_2$O$_{gas}$ at this level, and from the gas–liquid shift of 36 ppm[42]).

Results and Discussion

I. [WOH$_4$]

A. Structure and energies: As a simplified model system for tetramethyloxotungsten, we first consider the oxohydride [WOH$_4$]. Previous comparisons of d^0 hydrides and methyl compounds, for example between [WH$_6$] and [W(CH$_3$)$_6$][9, 12] or between [TaH$_5$] and [Ta(CH$_3$)$_5$],[7, 18] have shown that the smaller hydride ligand allows the adoption of more distorted structures. DFT preoptimizations without symmetry, starting from various different nuclear arrangements (e.g., square pyramidal, trigonal bipyramidal), generally converged to the severely distorted C_s-symmetrical structure **1C$_s$-1** (Figure 1a). It may be regarded as derived from a trigonal bipyramid with oxygen in the equatorial position by movement of the axial hydrogen atoms (H3, H3′) towards one of the two equatorial hydrogens (H1). Alternatively, starting from the regular square pyramid **1C$_{4v}$** (Figure 1c), two hydrogen atoms H3, H3′ in diagonal positions are also displaced towards H1. At the same time, the H3-W-O (and H3′-W-O) and H1-W-O angles are compressed, whereas the H2-W-O angle is expanded. The distortion is accompanied by a contraction of the W−H1 and W−H3 (W−H3′) distances, and by an expansion of the W−H2 distance (this differs from the situation for [WO(CH$_3$)$_4$], see below). Note that the H1−H3 distance is computed to be 1.695 Å, which is too large to assume any significant H···H bonding interactions.

Harmonic vibrational frequency analysis indicates that the regular square pyramidal structure **1C$_{4v}$** is a transition state

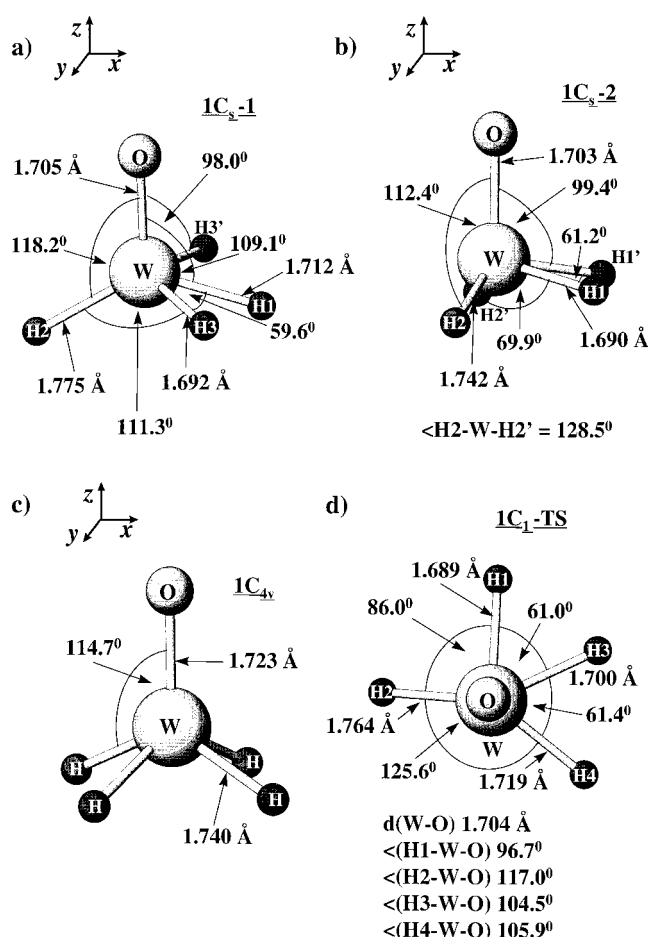Figure 1. Optimized stationary points for [WOH$_4$], with atom labeling and Cartesian coordinate system used for MO analyses. a) **1C$_s$-1** (minimum); b) **1C$_s$-2** (minimum); c) **1C$_{4v}$** (transition state with doubly degenerate imaginary frequency); d) **1C$_1$-TS** (transition state).

with a degenerate imaginary vibrational mode (cf. Table 1). It connects four equivalent minima **1C$_s$-1** (this E symmetry vibration is computed to have a force constant and frequency of −0.553 mDyne Å^{-1} and i944 cm^{-1}, respectively). In contrast, **1C$_s$-1** is characterized as a minimum with no low-energy vibrational modes (Table 1). An optimization in C_{2v} symmetry, starting from a regular trigonal bipyramid with oxygen in the equatorial position, converged to **1C$_{4v}$**. A trigonal bipyramidal structure **1C$_{3v}$** with oxygen in the axial position also is not competitive (Table 1).

Table 1. Relative energies (kJ mol^{-1}) for different stationary points on the [WOH$_4$], [WO(CH$_3$)$_4$], [ReOH$_4$], and [ReO(CH$_3$)$_4$] potential energy surfaces.[a]

| | [WOH$_4$] (**1**) | | | [WO(CH$_3$)$_4$] (**2**) | | | [ReOH$_4$] (**3**) | | | [ReO(CH$_3$)$_4$] (**4**) | |
structure	ΔE_{rel}[b]	N_{imag}[c]	structure	ΔE_{rel}[b]	N_{imag}[c]	structure	ΔE_{rel}[b]	N_{imag}[c]	structure	ΔE_{rel}[b]	N_{imag}[c]
1C$_s$-1	0.0 (0.0)	0	**2C$_s$-1**	0.0 (0.0)	0	**3C$_s$-1**	+11.7 (+7.2)	1 (A″)			
1C$_s$-2	+1.1 (+0.9)	0	**2C$_s$-2**	+2.6 (+2.2)	1 (A″)	**3C$_s$-2**	0.0 (0.0)	0			
1C$_{4v}$	+87.1 (+77.6)	2 (E)	**2C$_{4v}$-1**	+7.6 (+4.7)	2 (E)	**3C$_{4v}$**	+19.9 (+11.1)	2 (E)	**4C$_{4v}$-1**	0.0 (0.0)	0
1C$_{3v}$[d]	+142.7 (+136.2)	2 (E)	**2C$_s$-1b**	+2.7 (+3.0)	3 (A′,A″,A″)				**4C$_{4v}$-2**	44.2 (40.6)	2 (E)
1C$_1$-TS	+1.7 (+0.4)	1	**2C$_{4v}$-2**	+66.2 (+61.7)	6 (A$_2$,E,E,B$_1$)						
			2C$_{2v}$	+24.8 (+20.7)	4 (B$_2$,A$_2$,B$_1$,B$_1$)						

[a] DFT results. See Figures 1, 3, 5 for the structures of the stationary points considered. [b] Energies relative to the most stable structures **1C$_s$-1**, **2C$_s$-1**, and **3C$_s$-2**, respectively. Numbers in parentheses include zero-point vibrational energy corrections. Zero-point vibrational energies of 82.1, 374.5, and 85.2 kJ mol^{-1} were computed for **1C$_s$-1**, **2C$_s$-1**, and **3C$_s$-2**, respectively. [c] Number of computed imaginary harmonic vibrational frequencies and their symmetry assignment. Degenerate (E) modes are counted doubly. [d] Regular trigonal bipyramid with axial oxygen, see text.

However, in the DFT optimizations we found a second C_s minimum, **1C$_s$-2** (cf. Figure 1b), only ca. 1 kJmol^{-1} higher in energy than **1C$_s$-1** (Table 1). These two structures are thus almost degenerate energetically. **1C$_s$-2** is best described as a distorted square pyramid, in which the angle between two neighboring hydrogen atoms (H1, H1′) is decreased to about 70° and the one between the other two hydrogen atoms (H2, H2′) is increased to about 129° (the H1-W-H2 angle is thus also reduced significantly). The W−H1 (W−H1′) distances are diminished compared with **1C$_{4v}$**, whereas the W−H2 (W−H2′) distances are essentially unchanged. The H-W-O angles (in particular the H1-W-O angle) are all reduced, that is, the hydrogen atoms are moved up towards the xy plane containing the metal atom. The H1−H1′ distance of approximately 1.720 Å speaks against any significant H···H bonding (see above).

One can easily verify that the two sets of minima **1C$_s$-1** and **2C$_s$-1** must each exist in four equivalent orientations corresponding to permutations of the hydrogen atoms. In spite of the high energy of the degenerate transition state **1C$_{4v}$** (Table 1) for the interconversion of the different minima **1C$_s$-1**, the different sets of minima **1C$_s$-1** and **1C$_s$-2** may interconvert rapidly via unsymmetrical transition states **1C$_1$-TS** (Figure 1d). As **1C$_1$-TS** is computed to lie only ca. 1.7 kJmol^{-1} and 0.6 kJmol^{-1} above **1C$_s$-1** and **1C$_s$-2**, respectively, [WOH$_4$] is clearly predicted to be a highly fluxional molecule at room temperature. CCSD(T) single-point energy calculations place **1C$_s$-2** at +1.6 kJmol^{-1} and **1C$_{4v}$** at +70.1 kJmol^{-1} above **1C$_s$-1**, in good agreement with the DFT results (similar results are obtained at CCSD and MP2 levels, whereas Hartree – Fock energies would predict **1C$_s$-2** to be slightly below **1C$_s$-1**). However, the CCSD(T) single-point energy for **1C$_1$-TS** is approximately 0.9 kJmol^{-1} below that for **1C$_s$-2**. Furthermore, the energy differences between different stationary points are already reduced notably when only zero-point vibrational energy corrections are included (cf. numbers in parentheses in Table 1). Thus, probably not too much significance should be attached to the minimum character computed for **1C$_s$-2**.

A comparison with the recent ab initio calculations on [TaH$_5$][7] by Kang et al.[7] is instructive: While these authors found a regular square pyramid to be the lowest energy structure for this d^0 complex, equivalent C_{4v} minima may fluctuate via low-lying C_{2v} symmetrical transition states (recomputed at at the present DFT level to be at $\Delta E \approx$ +6 kJmol^{-1} above the regular square pyramid). The latter[7] are closely related to the lowest energy **1C$_s$-1** minima for [WOH$_4$] (in Figure 1a, imagine oxygen replaced by hydrogen, and add a second mirror plane containing W, H1, H3, and H3′). Thus, the relative roles of transition states and minima in the two types of systems appear simply to be reversed, owing to the presence of one π-donating oxo ligand in [WOH$_4$] (see below).

The structure **1C$_s$-1** of [WOH$_4$] may be related to the structure type denoted as edge-bridged tetrahedral by Ward et al.[25] for MX$_2$R$_3$ systems like [Cp$_2$TaH$_3$] (Cp = η^5-C$_5$H$_5$) when the H1 ligand in the present MXR$_4$ system is considered to bridge the H3−H3′ edge of the distorted tetrahedron formed by the O, H2, H3, and H3′ atoms (cf. Figure 1a). Thus,

the trend of a symmetry lowering due to the presence of one π-donor ligand as in [WOH$_4$] is apparently continued[25] for two π-donor ligands (see bonding discussion below). Such a straightforward relation to other known coordination environments appears to be difficult for structure **2C$_s$-2**.

B. Bonding: Within a simple one-electron frontier-orbital model, the distortions **1C$_{4v}$** → **1C$_s$-2** may be rationalized qualitatively in terms of improved metal – ligand orbital interactions in the lower symmetry structures, in analogy to previous discussions.[1, 5, 7, 11, 15, 18] Figure 2 shows an orbital correlation diagram for the distortions, based on the com-
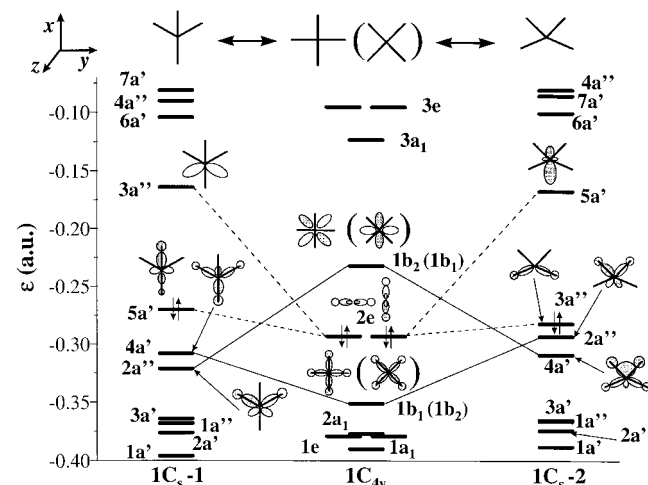

Figure 2. MO correlation diagram for the **1C$_{4v}$** → **1C$_s$-1** and **1C$_{4v}$** → **1C$_s$-2** distortions of [WOH$_4$]. The MO energies were extracted from the DFT calculations. Only a few of the major orbital correlations occuring upon lowering of symmetry are indicated by lines. Schematic MO drawings look down along the W−O axis. A nonconventional Cartesian coordinate system is used for C_s symmetry (with the W−O bond along the z axis), as well as for the 45°-rotated representation of **1C$_{4v}$** (right side). Note that b$_1$ and b$_2$ symmetry are switched in the rotated structure (cf. labels in parentheses). The HOMOs are indicated by vertical arrows for electron spin.

puted Kohn – Sham orbitals. MOs for regular square pyramidal transition metal complexes have been studied in detail previously by many workers. The relation to other coordination geometries and the dependence on the pyramidalization angle have received most attention,[7, 14, 15, 18, 25] but the effect of σ- and π-donor ligands at various coordination sites was also considered.[14, 25] We start the correlation **1C$_{4v}$** → **1C$_s$-1** in the conventional orientation for C_{4v} symmetry, with the hydrogen atoms on the xz and yz planes, whereas an orientation rotated by 45° is used for the correlation with **1C$_s$-2**. The C_s structures are both oriented nonconventionally (with the W−O bond along the z axis) for comparison. Owing to the low symmetry of **1C$_s$-1** and **1C$_s$-2**, many metal d orbitals and ligand orbitals may interact in the distorted structure (depending only on whether or not they are symmetrical or antisymmetrical with respect to the unique mirror plane). In each case we have only indicated the most significant orbital correlations in Figure 2. Note also that the simplified MO drawings concentrate on the W−H interactions (roughly parallel to the xy plane), whereas some of the MOs are also

involved in significant W–O interactions in the z direction (see discussion below).

One very important electronic aspect in the regular square pyramidal structure is the presence of an unoccupied low-energy nonbonding metal d_{xy} orbital ($1b_2$ LUMO), which finds no appropriate ligand orbital combination with which it may interact. In contrast, the metal $d_{x^2-y^2}$ orbital is ideally suited in $1C_{4v}$ to form bonds to the hydride ligands in the basal plane, resulting in a low-energy W–H bonding MO of $1b_1$ symmetry (d_{xy} and $d_{x^2-y^2}$ character, and thus b_1 and b_2 symmetry are switched in the $45°$ rotated orientation, right side of Figure 2). Further W–H bonding interactions are connected to the $2e$ MOs. The two components of this degenerate set feature, respectively, contributions from metal $d_{xz}p_x$ and $d_{yz}p_y$ hybrids. In spite of this hybridization towards the basal hydrides, away from the apical oxo ligand, these MOs are still to some extent $\pi(W–O)$ antibonding, an important feature discussed below. Four other valence MOs ($\pi(W–O)$, $\sigma(W–O)$, and W–H bonding) are at lower energies.

Let us first consider the distortion $1C_{4v} \rightarrow 1C_s\text{-}1$ (left side of Figure 2): The metal d_{xy} AO may now contribute significantly to W–H3 (W–H3′) bonding within the $2a''$ MO (including some bonding admixture by one of the components of the former $2e$ set). This may be considered a major driving force for distortion (however, see below). In contrast, the bonding interactions of the $d_{x^2-y^2}$ AO are diminished, and therefore the corresponding MO (now $4a'$) is destabilized. This change disfavors the distortion. An antibonding admixture of some s, p_x, and d_{xz} character (cf. former $2e$ set) to the former $1b_2$ MO gives the $5a'$ HOMO. The $3a''$ LUMO is at relatively high energy and derives from an antibonding d_{xy} admixture to the other of the two former $2e$ components.

A complementary picture is found for the $1C_{4v} \rightarrow 1C_s\text{-}2$ distortion (right side of Figure 2): The metal $d_{x^2-y^2}$ AO now contributes in a significantly bonding fashion to the $4a'$ MO, providing a major driving force to the energy lowering. In contrast, the former $1b_2$ MO (with metal d_{xy} character) is destabilized ($2a''$ MO), as the overlap with the H2 and H2′ orbitals is diminished. The $3a''$ HOMO corresponds to an appropriate linear combination of the components of the former $2e$ set (slightly destabilized), whereas the high-energy $5a'$ LUMO is an antibonding combination of former $2e$ and $1b_1$ components. Again, a major effect of the symmetry lowering is the removal of the low-lying LUMO.

We have discussed above how, in simple homoleptic d^0 MR_5 systems like [TaH$_5$], the regular square pyramidal structure is favored, whereas distorted edge-bridged tetrahedral[25] C_{2v} structures analogous to $1C_s\text{-}1$ show up only as low-lying transition states.[7] Thus, the improved involvement of the d_{xy} AO in bonding at lower symmetry is not quite sufficient to offset the unfavorable changes in other interactions (in particular in those involving the $d_{x^2-y^2}$ AO). How does the presence of the π-donor oxo ligand in the apical position tip the balance in favor of the low-symmetry structures? The answer is related to the above-mentioned $\pi(W–O)$-antibonding nature of the $2e$ set in $1C_{4v}$. In $1C_s\text{-}1$, this antibonding contribution is reduced significantly, as one component of the former $2e$ set now dominates the $3a''$ LUMO and is thus unoccupied. Similarly in $1C_s\text{-}2$, $\pi(W–O)$-antibonding charac-

ter is removed, as part of the former $2e$ set now contributes to the $5a'$ LUMO. It is notable in this context that the W–O distance contracts by ca. 0.01 Å upon distortion (cf. Figure 1).

One structural consequence of the reduced π-antibonding in the distorted structures is that, besides the distortions within the basal plane, the hydrogen atoms H1, H3, and H3′ in $1C_s\text{-}1$ and the hydrogen atoms H1 and H1′ in $1C_s\text{-}2$ are moved up towards the xy plane containing the metal atom, and may now interact better with the corresponding in-plane metal AO (cf. H-W-O angles in Figure 1). Such a dependence of π interactions on the pyramidalization angle has also been discussed previously for the regular square pyramid.[14]

We may compare these results to those obtained for the MX_2R_3 case by Ward et al.:[25] In each case in which a so-called edge-bridged tetrahedral arrangement (analogous to $1C_s\text{-}1$) is preferred over a regular square pyramid, this is accompanied by diminished $\pi(M–X)$ antibonding interactions. In other words, the σ-donor ligands are arranged such that competition with π donation is minimized. Thus, while improved M–R σ-bonding is an important driving force towards lower symmetry, as discussed above, these interactions alone do not appear to be sufficient to effect the distortion and thus to overcome the increased ligand repulsion in the distorted structures. However, these interactions certainly prepare the ground for relatively shallow potential energy surfaces.

These considerations are confirmed by results of natural population and natural localized MO analyses (NPA, NLMO) for $1C_s\text{-}1$, $1C_s\text{-}2$, and $1C_{4v}$ (Table 2). As expected, the distortion increases the natural atomic orbital (NAO) metal d population $d(W)$ and thus reduces the positive metal charge $Q(W)$ considerably. More specifically, the nonbonding d_{xy} NAO (cf. the $1b_1$ MO in conventional orientation), which is not populated in $1C_{4v}$, becomes significantly populated in $1C_s\text{-}1$. The same holds for the $d_{x^2-y^2}$ AO in $1C_s\text{-}2$ (note the rotated orientation for $1C_{4v}$ in Figure 2). The d_{yz} population in $1C_s\text{-}1$ and the d_{xz} population in $1C_s\text{-}2$ are reduced significantly compared with $1C_{4v}$, consistent with the above-mentioned removal of $\pi(W–O)$-antibonding interactions.

Within a natural localized molecular orbital (NLMO) framework, covalent contributions to the (contracted, cf. Figure 1a) W–H1, W–H3, and W–H3′ bonds increase for $1C_s\text{-}1$ compared with $1C_{4v}$. The same holds for the W–H1 and W–H1′ bonds in $1C_s\text{-}2$. In contrast, the covalency of the expanded W–H2 bond in $1C_s\text{-}1$ and of the W–H2 and W–H2′ bonds in $1C_s\text{-}2$ decreases, with a concomitant decrease of the metal d character used for the bond. These results fit nicely into the general picture of increased covalency for some of the bonds in the distorted structures at the expense of other bonds, as discussed previously for [WH$_6$] and [W(CH$_3$)$_6$].[6] In all cases, the overall covalency increases upon distortion. Most notably, the $\pi(W–O)$ NLMOs become much more covalent upon distortion, in particular the $\pi_y(W–O)$ NLMO in $1C_s\text{-}1$, and the $\pi_x(W–O)$ NLMO in $1C_s\text{-}2$. This also supports a removal of $\pi(W–O)$ antibonding character upon distortion.

II. [WO(CH$_3$)$_4$]

A. Structure and energies: For the methyl complex [WO(CH$_3$)$_4$] (**2**), different conformational orientations of

Table 2. Natural populations and charges (Q), and analysis of natural localized molecular orbitals (NLMO) for different stationary points of [WOH$_4$].[a]

		1C$_s$-1[b]		**1C$_s$-2**[b]		**1C$_{4v}$**
NPA	Q(W)	+ 0.966	Q(W)	+ 0.964	Q(W)	+ 1.428
	s(W)	0.685	s(W)	0.630	s(W)	0.711
	p(W)	0.036	p(W)	0.036	p(W)	0.060
	d$_{xy}$(W)	0.805	d$_{xy}$(W)	1.373	d$_{xy}$(W)	0.000
	d$_{xz}$(W)	0.863	d$_{xz}$(W)	0.615	d$_{xz}$(W)	0.920
	d$_{yz}$(W)	0.597	d$_{yz}$(W)	0.830	d$_{yz}$(W)	0.920
	d$_{x^2-y^2}$(W)	1.351	d$_{x^2-y^2}$(W)	0.869	d$_{x^2-y^2}$(W)	1.304
	d$_{z^2}$(W)	0.697	d$_{z^2}$(W)	0.683	d$_{z^2}$(W)	0.657
	d$_{tot}$(W)	4.313	d$_{tot}$(W)	4.370	d$_{tot}$(W)	3.801
	Q(O)	− 0.489	Q(O)	− 0.488	Q(O)	− 0.608
	Q(H1)	− 0.095	Q(H1, H1′)	− 0.036	Q(H)	− 0.213
	Q(H2)	− 0.298	Q(H2, H2′)	− 0.222		
	Q(H3,H3′)	− 0.061				
NLMOs[c]	σ(W−O)	27%,92% d	σ(W−O)	27%,94% d	σ(W−O)	27%,94% d
	π$_x$(W−O)	13%, 100% d	π$_x$(W−O)	27%, 98% d	π$_x$(W−O)	12%,96% d
	π$_y$(W−O)	27%,100% d	π$_y$(W−O)	21%, 99% d	π$_y$(W−O)	12%,96% d
	W−H1	48%,94% d	W−H1 (W−H1′)	49%, 88% d	W−H	44%,80% d
	W−H2	39%,69% d	W−H2 (W−H2′)	39%, 76% d		
	W−H3 (W−H3′)	48%,82% d				

[a] Based on the Kohn–Sham wavefunction. Charges do not add up exactly to 0, as the slight depletion of some metal semicore orbitals has been neglected. [b] Molecular orientation for **1C$_s$-1** and **1C$_s$-2** chosen unconventionally (see Figure 1) to facilitate comparison with **1C$_{4v}$**. [c] The relative metal character of a given NLMO, and the relative d-orbital contributions to this metal character are given.

the methyl groups are feasible, which may differ considerably in energy as a result of conformation-dependent agostic interactions.[9, 12, 18, 43] Several stationary points on the potential energy surface thus have been considered (cf. Figure 3). Computed relative DFT energies are given in Table 1. Structure parameters for **2C$_s$-1**, **2C$_s$-2**, **2C$_{4v}$-1**, and **2C$_{4v}$-2** are given in Tables 3 – 5 (data for **2C$_s$-1b** and **2C$_{2v}$** may be found in Tables S1 and S2 in the supporting information). As for the hydride, the regular square pyramidal structures (**2C$_{4v}$-1** and **2C$_{4v}$-2**, cf. Figure 3c,e) are no minima. However, while conformation **2C$_{4v}$-2**, with the axial hydrogen atoms synperiplanar to the oxo ligand, is very high in energy (66.2 kJ mol^{-1} above **2C$_s$-1**) and is characterized as a higher order saddle

point (with four imaginary modes), the antiperiplanar conformation **2C$_{4v}$-1** is considerably more stable (only 7.6 kJ mol^{-1} above **2C$_s$-1**). It has only one degenerate (E) imaginary mode, and therefore corresponds closely to the transition state **1C$_{4v}$** of the hydride. Thus, in these regular square pyramidal structures, the rotation around the C−W single bonds appears to be strongly hindered. Comparably large energy differences between all-*anti* and all-*syn* arrangements of the basal methyl groups in a square pyramidal d^0 complex have been found computationally for [Ta(CH$_3$)$_5$] by Albright and Tang (51.4 kJ mol^{-1} at MP2 level).[15]

The lowest energy minimum **2C$_s$-1** for [WO(CH$_3$)$_4$] (see Figure 3a) is analogous to **1C$_s$-1** for [WOH$_4$] (cf. Figure 1a),
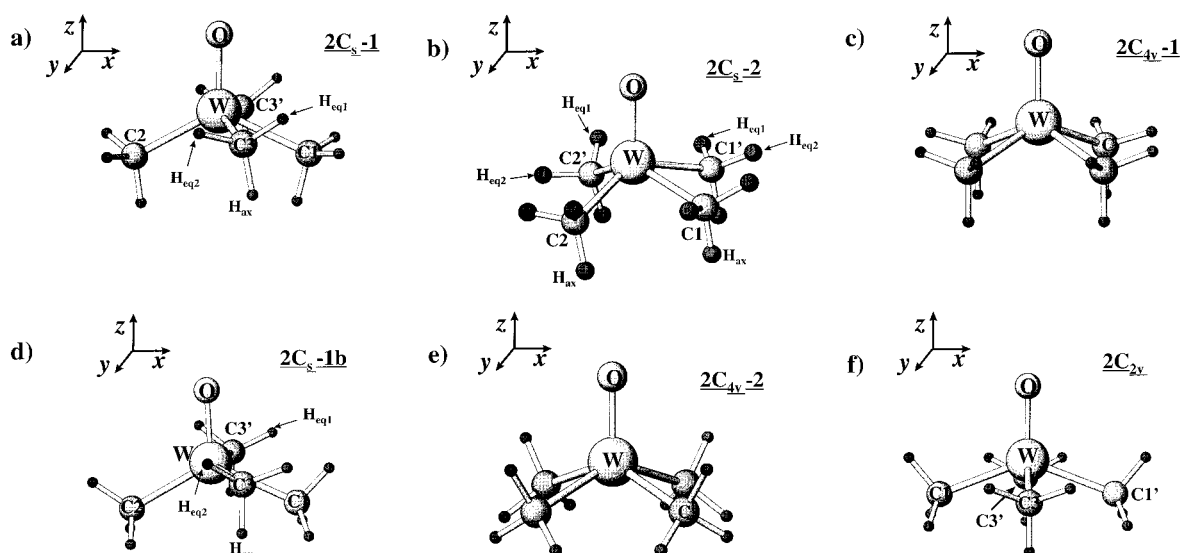

Figure 3. Stationary points considered for [WO(CH$_3$)$_4$], with atom labeling and Cartesian coordinate system used for MO analyses. a) **2C$_s$-1**, all axial hydrogen atoms antiperiplanar to oxygen; b) **2C$_s$-2**; c) **2C$_{4v}$-1**, all axial hydrogen atoms antiperiplanar to oxygen; d) **2C$_s$-1b**, axial hydrogen atoms at C1 and C2 synperiplanar to oxygen; e) **2C$_{4v}$-2**, all axial hydrogen atoms synperiplanar to oxygen; f) **2C$_{2v}$**, axial hydrogen atoms at C1, C1′ synperiplanar to oxygen.

Table 3. Predicted structural parameters for **2C$_s$-1**.[a]

W–O	1.726	C3–H$_{ax}$	1.105	H$_{ax}$-C1-W	102.3
W–C1	2.227	C3–H$_{eq1}$	1.103	H$_{eq}$-C1-W	115.5
W–C2	2.140	C3–H$_{eq2}$	1.116	H$_{ax}$-C2-W	111.7
W–C3	2.152	C1-W-O	116.8	H$_{eq}$-C2-W	111.3
C1–H$_{ax}$	1.114	C2-W-O	118.4	H$_{ax}$-C3-W	114.0
C1–H$_{eq}$	1.103	C3-W-O	98.1	H$_{eq1}$-C3-W	115.3
C2–H$_{ax}$	1.109	C3-W-C1	73.7	H$_{eq2}$-C3-W	101.2
C2–H$_{eq}$	1.109	C3-W-C2	98.4		

[a] Distances A–B in Å, angles A-B-C in ° (see Figure 3a).

Table 4. Predicted structural parameters for **2C$_s$-2**.[a]

W–O	1.728	C1-W-O	104.8
W–C1	2.200	C2-W-O	113.6
W–C2	2.144	C1-W-C1′	74.3
C1–H$_{ax}$	1.107	C2-W-C2′	99.2
C1–H$_{eq1}$	1.107	C1-W-C2	79.9
C1–H$_{eq2}$	1.103	H$_{ax}$-C1-W	109.9
C2–H$_{ax}$	1.106	H$_{eq1}$-C1-W	109.1
C2–H$_{eq1}$	1.106	H$_{eq2}$-C1-W	113.1
C2–H$_{eq2}$	1.117	H$_{ax}$-C2-W	115.6
		H$_{eq1}$-C2-W	113.4
		H$_{eq2}$-C2-W	104.0

[a] Distances A–B in Å, angles A-B-C in ° (see Figure 3b).

Table 5. Predicted structural parameters for **2C$_{4v}$-1** and **2C$_{4v}$-2**.[a]

	2C$_{4v}$-1	**2C$_{4v}$-2**
W–O	1.737	1.731
W–C	2.166	2.193
C–H$_{ax}$	1.106	1.110
C–H$_{eq}$	1.108	1.103
C-W-O	111.3	107.9
C-W-C (cis)	82.4	84.6
H$_{ax}$-C-W	112.1	105.8
H$_{eq}$-C-W	110.5	114.6

[a] Distances A–B in Å, angles A-B-C in ° (see Figures 3c,e).

and features similar distortions (see Table 3). However, there are some significant structural differences: a) The C3-W-C1 angle in **2C$_s$-1** is compressed considerably less (73.7° vs. 59.6°) than the H3-W-H1 angle in **1C$_s$-1**. b) The C1-W-O angle is expanded rather than compressed relative to that in **2C$_{4v}$-1**. c) The W–C1 distance is expanded rather than contracted. Related differences between the structural distortions found for hydride and methyl analogues were noted for [WH$_6$] and [W(CH$_3$)$_6$],[9] and are at least partially related to the much larger ligand–ligand repulsions in the methyl species, and to agostic C–H→M interactions (see below).

In contrast to [WOH$_4$], at this computational level the second type of distorted C_s structure, **2C$_s$-2** (Figure 3b, Table 4), is no minimum but a low-lying transition state for interconversion of **2C$_s$-1** (Table 1). The overall distortions of **2C$_s$-2** are similar to those for the hydride, and the computed energy is only ca. 3 kJ mol^{-1} above **2C$_s$-1**. However, the structure of the methyl compound (**2C$_s$-2** vs. **2C$_{4v}$-1**) is again less distorted than that of the hydride (**1C$_s$-2** vs. **1C$_{4v}$**). In particular, the W–C1 (W–C1′) distances pertaining to the compressed C1-W-C1′ (and C1-W-C2) angle are expanded compared with those in **2C$_{4v}$-1**. This contrasts to **1C$_s$-2** but is consistent with the differences between **2C$_s$-1** and **1C$_s$-1**, and

between [W(CH$_3$)$_6$] and [WH$_6$].[6] In all cases, those W–C distances in the methyl compounds belonging to the compressed angles are extended compared with the high-symmetry structures, whereas the opposite holds true for the W–H distances in the analogous hydride structures.

Most notably, **2C$_{4v}$-1** is much more competitive with **2C$_s$-1** and **2C$_s$-2** than **1C$_{4v}$** is with **1C$_s$-1** and **1C$_s$-2** (ca. 8 kJ mol^{-1} vs. ca. 87 kJ mol^{-1}). This is again consistent with previous comparisons between methyl complexes and hydride model systems.[7, 9] Thus, in contrast to [WOH$_4$], at room temperature [WO(CH$_3$)$_4$] is expected to fluctuate even via the low-lying degenerate transition state **2C$_{4v}$-1** (the imaginary E vibrational mode of **2C$_{4v}$-1** is computed to have a force constant and frequency of only − 0.070 mDyne Å^{-1} and i143 cm^{-1}, respectively). In any case, [WO(CH$_3$)$_4$] is also predicted to be a highly fluxional molecule, but with a somewhat different character of the potential energy surface than its hydride analogue. As discussed above for the latter, the energy differences between different structures are further reduced when zero-point vibrational energy corrections are included (Table 1).

Interestingly, the rotation of the two methyl groups 1 and 2 in **2C$_s$-1** into a synperiplanar orientation (**2C$_s$-1**→**2C$_s$-1b**, Figure 3) costs considerably less energy (2.7 kJ mol^{-1}) than expected on the basis of the rather large **2C$_{4v}$-1** vs. **2C$_{4v}$-2** energy difference (66.2 kJ mol^{-1}), or from the related reorientation of just two methyl groups from **2C$_{4v}$-1** (17.2 kJ mol^{-1}, cf. Table 1). Thus, apparently the rotation of these two methyl groups is considerably easier[44] than in the regular square pyramid. In contrast, a partial optimization with the 'axial' H-C3-W-O (H-C3′-W-O) dihedral angles fixed at 0° (in the fully optimized structure **2C$_s$-1**, the corresponding 'axial' hydrogen dihedral angle is 172.8°) leads to an energy increase by ca. 16.5 kJ mol^{-1}, comparable to that for the **2C$_{4v}$-1**→**2C$_{2v}$** transformation. Similarly, in **2C$_s$-2** a corresponding partial optimization, with the axial hydrogens on C1, C1′ fixed to a synperiplanar arrangement towards oxygen, causes an energy increase of 24.2 kJ mol^{-1}, whereas the corresponding synperiplanar arrangement for methyl groups 2 and 2′ is only ca. 9.2 kJ mol^{-1} above **2C$_s$-2**.

B. Agostic interactions: Albright and Tang had attributed the conformational energy differences in [Ta(CH$_3$)$_5$] largely to repulsions between neighboring hydrogen atoms.[15] However, we have reason to believe that the rotational barriers, and the unusually strong coupling of the methyl group rotation to the distortional modes in [WO(CH$_3$)$_4$], are at least in part related to significant agostic interactions.[43] Thus, for example, the barriers are significantly reduced in the d^1 complex [ReO(CH$_3$)$_4$], in spite of even shorter H···H distances (see below). Hyperconjugative C–H→W interactions are apparent from the C–H distances and H-C-W angles summarized in Tables 3–5, and from the natural population analyses (see discussion below). Thus, for example, the axial C–H bonds in the synperiplanar arrangement **2C$_{4v}$-2** act as significant agostic donors, as evidenced by the large C–H distances and small H-C-W angles (Table 5), whereas the equatorial C–H bonds do not contribute significantly (they are contracted and have larger angles[45]). In contrast, in the antiperiplanar structure

2C$_{4v}$-1 (Figure 3c), all hydrogen atoms apparently interact almost equally well with empty metal orbitals, leading to almost uniform C–H distances and H-C-W angles. This contributes significantly to the much lower energy of **2C$_{4v}$-1** compared with **2C$_{4v}$-2** (cf. Table 2).

Closer inspection of the C–H distances and H-C-W angles in the lowest energy structure **2C$_s$-1** indicates that, for example, agostic interactions for methyl group 3 (3′) are largely due to the C3–H$_{eq2}$ bond (cf. Table 3). This may be rationalized with the shape of the 3a″ LUMO acting as the major acceptor for hyperconjugation (Figure 2, left). In contrast, the C1–H$_{ax}$ bond is the most important agostic donor for methyl group 1, whereas the distribution is rather uniform for methyl group 2. In **2C$_s$-2**, the agostic interactions in methyl groups 1, 1′ are almost uniformly distributed over the C1–H$_{ax}$ and C1–H$_{eq1}$ bonds, whereas the dominant agostic interactions for methyl groups 2, 2′ are due to the C2–H$_{eq2}$ bond (cf. 5a′ LUMO in Figure 2, right). Thus, there is a strong conformational dependence of the C–H→W donor interactions, consistent with the computed rotational barriers. Generally, an antiperiplanar orientation of the methyl groups with respect to the oxo ligand is favored over a synperiplanar one. However, the energy gain and the structural changes due to such an arrangement obviously depend on the orientation of a given group with respect to the potential acceptor orbitals at the metal.

Do the agostic interactions favor or oppose the low-symmetry distortions? In the case of [W(CH$_3$)$_6$], partial optimizations with frozen, idealized methyl group structures indicated that the agostic interactions may add to the preference for a skeletal distortion from D_{3h} to C_{3v}.[9] For [WO(CH$_3$)$_4$], we have carried out the same rough test, by doing partial optimizations with all methyl groups fixed to local C_{3v} symmetry, with d(C–H) = 1.107 Å and ∡(H-C-W) = 110.8°. The energy increase with respect to the corresponding fully optimized structures is 7.3, 4.3, 0.5, and 8.1 kJ mol^{-1} for **2C$_s$-1**, **2C$_s$-2**, **2C$_{4v}$-1**, and **2C$_{4v}$-2**, respectively. This would suggest that the **2C$_{4v}$-1** → **2C$_s$-1** and **2C$_{4v}$-1** → **2C$_s$-2** distortions may be slightly facilitated by the agostic interactions. However, the same measure would predict **2C$_{4v}$-2** to have larger agostic interactions than **2C$_{4v}$-1**; this is inconsistent with the lower energy (and larger d$_{xy}$ populations, see below) of **2C$_{4v}$-1**. This is due to the fact that the C–H distances and H-C-W angles are much more uniform in **2C$_{4v}$-1** than in **2C$_{4v}$-2** (Table 5). Therefore, this type of test may not be adequate for an assessment of the energy stabilization by the agostic delocalizations, but rather indicate the magnitude of the structural deformations of the methyl groups. A different, semiquantitative measure of the energy stabilization due to agostic interactions is offered by a second-order perturbation theoretical analysis of delocalization interactions within the framework of the strictly localized natural bond orbitals.[35] The results suggest that the agostic interactions increase upon distortion, owing to a larger number of hyperconjugatively interacting NBOs in the lower symmetry structures. Nevertheless, we have to conclude at present that none of the available analysis schemes provides a definite answer to whether or not the agostic delocalizations favor the symmetry distortions of the heavy-atom skeleton.

C. Other bonding features: Differences in structure and bonding of the methyl complex with respect to the hydride arise from several factors (see also above): a) the larger size of the methyl ligands, b) the possibility of C–H→W agostic interactions (see also the discussion above), c) the more directional bonding possible with sp^n hybrid orbitals for methyl ligands compared with the hydrogen 1s orbitals in the hydrides, d) differences in the electronegativities of methyl and hydride ligands. At least factor a) will lead to a reduced preference for distortion in the methyl compound. Whether the same holds true for factor b) is not answered easily, as evidenced by the discussion above and by that in ref. [9].

Inspection of the Kohn–Sham MOs (MO energies given in Table S3 of supporting information) indicates that the b$_2$-type LUMO (cf. MO diagram for [WOH$_4$] in Figure 2) in the regular square pyramidal structure **2C$_{4v}$-1** of [WO(CH$_3$)$_4$] is not as low in energy (with respect to the energies of the highest occupied MOs) as in the hydride (**1C$_{4v}$**). Within the framework of second-order perturbation theory, this suggests a reduced energy gain from distortion to lower symmetry, consistent with the computed energies (cf. Table 1). The LUMO is somewhat lower in energy for the less stable synperiplanar conformer **2C$_{4v}$-2**.

Indeed, natural population analysis shows (numerical data given in Table S4 of supporting information) that the d$_{xy}$ NAO is already significantly populated in **2C$_{4v}$-2**, and particularly in **2C$_{4v}$-1**, in contrast to **1C$_{4v}$** (cf. Table 2). This is due to agostic C$_{eq}$–H→d$_{xy}$(W) donor interactions (the b$_2$ LUMO has significant coefficients on the equatorial hydrogen atoms). These interactions appear to be more efficient for **2C$_{4v}$-1** than for **2C$_{4v}$-2**, and thus contribute to the computed large rotational barrier. The agostic interactions are also apparent from tails of the C–H bonding NLMOs at the metal. These follow roughly the C–H distances and H-C-W angles discussed above.

In spite of the agostic interactions present for the methyl compound, the positive metal charge is larger in **2C$_{4v}$-1** [Q(W) = +1.673] than in **1C$_{4v}$** [Q(W) = 1.428], indicating a larger electronegativity of methyl than hydride ligands. In addition to the larger size of the methyl groups, this larger bond ionicity enhances the ligand–ligand repulsions and the energy differences between occupied and unoccupied MOs (see above), and thus is expected to disfavor the distortion. In contrast, the oxygen charge is slightly lower in the methyl species, that is, the oxo ligand may withdraw less charge from the metal. As a consequence of the much smaller structural deviations from the regular square pyramid (**2C$_s$-1** vs. **1C$_s$-1** and **2C$_s$-2** vs. **1C$_s$-2**), the reduction of the metal charge upon symmetry lowering is considerably less for [WO(CH$_3$)$_4$] than for [WOH$_4$]. Thus, **2C$_s$-1** and **2C$_s$-2** are still considerably ionic (with NPA metal charges of +1.473 and +1.554, respectively). The corresponding changes in the d populations upon distortion are consequently also less dramatic. Still, except for the agostic interactions discussed above, the overall description is qualitatively similar to that given above in more detail for the hydride.

D. Vibrational frequency analyses: A simulated IR spectrum derived from the harmonic vibrational frequency analysis for the **2C_s-1** minimum of [WO(CH_3)_4] is shown in Figure 4a, together with a rough assignment of the vibrational
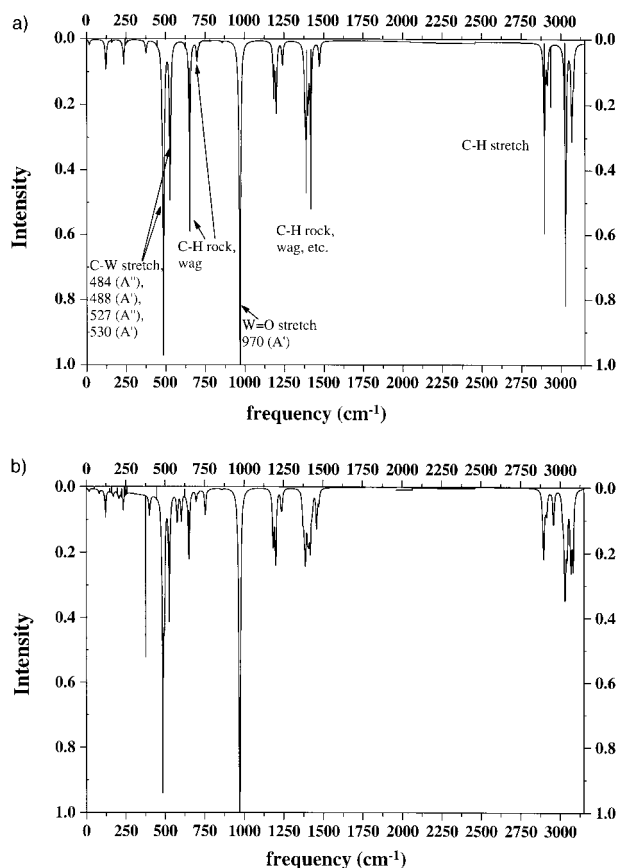

a)

b)

Figure 4. Simulated IR spectra for [WO(CH_3)_4]. The computed harmonic vibrational frequencies and intensities were convoluted using Lorenzians of half-width 10 cm^{-1}. Intensities have been scaled to that of the most intense band. a) **2C_s-1**; some assignments are indicated by arrows; b) superposition of computed spectra for **2C_s-1** and **2C_s-2** (the imaginary frequency for **2C_s-2** was deleted).

modes. As a result of the low symmetry, the spectrum is notably more complicated than the corresponding spectrum calculated for the regular square pyramidal structure **4C_4v-1** of [ReO(CH_3)_4] shown in Figure 5. In particular, the bands at ca. 485 cm^{-1} and ca. 530 cm^{-1} (asymmetric and symmetric W−C stretching modes) in **2C_s-1** are considerably more intense than the Re−C stretching modes for the rhenium complex, owing to the somewhat larger bond polarity. Moreover, the relative intensities of the C−H rocking type modes at ca. 600–720 cm^{-1} are switched in favor of the lower frequency band (which is quite intense). The structure of the C−H stretching bands between 2900 and 3100 cm^{-1} is also considerably more complicated as a result of the lower symmetry.

The transition state **2C_s-2** is very low in energy. What if it were another minimum, such as **1C_s-2**, other than is actually found computationally at this level? Figure 4b shows a superposition of the computed spectra for **1C_s-1** and **1C_s-2** with equal weights, using the same Lorenzian half width of 10 cm^{-1}. While the plot is clearly quite convoluted, the results
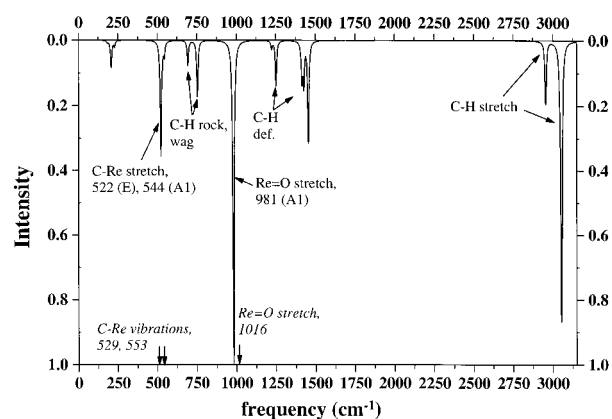

Figure 5. Simulated IR spectrum for [ReO(CH_3)_4] (**4C_4v-1**) (see legend of Figure 4). Some experimental assignments (ref. [21c]) are in italics, theoretical assignments in normal letters.

suggest that with reasonable spectral resolution and sample purity, the appearance of the spectrum is still characteristic of the low-symmetry distortions. IR spectroscopy at low temperatures[46] might thus be an appropriate means of experimentally confirming the predicted low-symmetry structure of [WO(CH_3)_4]. Note that the computed spectrum for [ReO(CH_3)_4] agrees well with the available experimental data.[21c]

E. NMR chemical shifts: Table 6 gives the computed isotropic carbon and oxygen NMR chemical shifts for the structures **2C_s-1**, **2C_s-2**, and **2C_4v-1** of [WO(CH_3)_4]. As expected, the carbon shifts for the distorted structures **2C_s-1** and **2C_s-2** vary

Table 6. Predicted isotropic ^{13}C and ^{17}O NMR chemical shifts (δ) for different structures of [WO(CH_3)_4].[a]

	2C_s-1		2C_s-2		2C_4v-1
O	+745	O	+673	O	+586
C1	+41	C1, C1′	+45	C	+50
C2	+39	C2, C2′	+51		
C3, C3′	+52				

[a] See Figure 3 for the atom labeling. Carbon shifts vs. TMS, oxygen shifts vs. H_2O_liq.

for the different coordination positions, whereas they are required by symmetry to be equal for the regular square pyramid **2C_4v-1**. However, in view of the computed low barriers for fluctuation, only averaged shifts will most likely be observable (in the range of ca. $\delta = 45–50$), probably even down to relatively low temperatures. The same holds for the ^{1}H shifts, for which the average computed values are ca. $\delta = +1.50$ for **2C_s-2** and **2C_4v-1**, and ca. $\delta = +1.35$ for **2C_s-1**. Thus, neither the ^{1}H nor the ^{13}C NMR chemical shifts seem to offer much potential for experimental confirmation of the predicted low-symmetry structures.

However, it appears that the oxygen shifts may be more useful in this respect. They are notably larger for the distorted structures **2C_s-1** and **2C_s-2** than for **2C_4v-1**. In view of the larger HOMO–LUMO gap in the distorted structures, this is at first sight surprising (however, note the lower negative charge on oxygen). Table 7 gives the computed oxygen shift tensors. The

Table 7. Predicted ^{17}O shift tensors (δ relative to H_2O_{liq}) for different structures of $[WO(CH_3)_4]$.[a]

	2C$_s$-1		2C$_s$-2		2C$_{4v}$-1
δ_{11} (δ_{xx})	+1268	δ_{11} (δ_{yy})	+1038	$\delta_{11} = \delta_{22}$	+871
δ_{22} (δ_{yy})	+773	δ_{22} (δ_{xx})	+880		
δ_{33} (δ_{zz})	+195	δ_{33} (δ_{zz})	+101	δ_{33} (δ_{zz})	+15
δ_{iso}	+745		+673		+586

[a] See Figure 3 for the atom labeling and Cartesian coordinates.

tensors have lost their axial symmetry in **2C$_s$-1** and **2C$_s$-2**, compared with the axially symmetrical tensor in **2C$_{4v}$-1**, with the σ_{11} component being more deshielded than in **2C$_{4v}$-1**. However, even the component parallel to the W–O axis (σ_{33}) becomes notably deshielded upon distortion.

MO analyses show that the π^*(W–O)-type unoccupied orbitals are lowered in energy. Thus, e.g. in the model system $[WOH_4]$, the π^*(W–O) character is concentrated in the high-lying 3e MO for **1C$_{4v}$**, whereas even the LUMOs have significant π^*(W–O) character in **1C$_s$-1** and **1C$_s$-2** (see discussion in Section I.B and Figure 2). This gives considerably increased paramagnetic contributions from magnetic-field induced π(W–O) → π^*(W–O) and σ(W–O) → π^*(W–O) couplings (see ref. [47] for more detailed analyses of oxygen shielding tensors in transition-metal oxo complexes). Thus the partial removal of π(W–O) antibonding interactions accounts largely for the increased ^{18}O shifts. The different orientations of δ_{11} for **2C$_s$-1** and **2C$_s$-2** in Table 7 are indeed fully consistent with the π-bonding discussion in section I.B.

In a fluxional structure, the statistical weights of the four minima **2C$_s$-1** and of the low-lying transition states **2C$_s$-2** will be largest, and these areas on the potential energy surface should dominate the averaged oxygen shifts. When taking the average of the two shift values for **2C$_s$-1** and **2C$_s$-2**, we arrive at a predicted average shift of $\delta \approx 710$, which is more than 120 ppm larger than the value computed for the regular structure **2C$_{4v}$-1**. As such a difference is expected for this system to lie significantly outside the systematic errors of the DFT methods used,[47] the large oxygen NMR chemical shifts might be useful as indirect indicators for the distorted, fluxional structure. This approach appears to be promising in view of the increasing use of ^{17}O NMR spectroscopy for organometallic oxo compounds.[48]

III. [ReOH$_4$]

A. Structure and energies: Compared with $[WOH_4]$, the rhenium oxohydride **3** has one more electron. Previous studies have shown that such d^1 systems may have a reduced tendency to distort to lower symmetries than their d^0 counterparts, provided the additional electron occupies an orbital which becomes destabilized upon symmetry lowering. Thus, $[Re(CH_3)_6]$, for example, is computed to exhibit a regular trigonal prismatic structure as opposed to the distorted one for $[W(CH_3)_6]$.[9, 12, 49]

Indeed, $[ReOH_4]$ is less distorted than $[WOH_4]$, as may be inferred from the relative energies for the stationary points in Table 1, and from the structural results shown in Figure 6. Most notably, **3C$_s$-1** is not computed to be a minimum

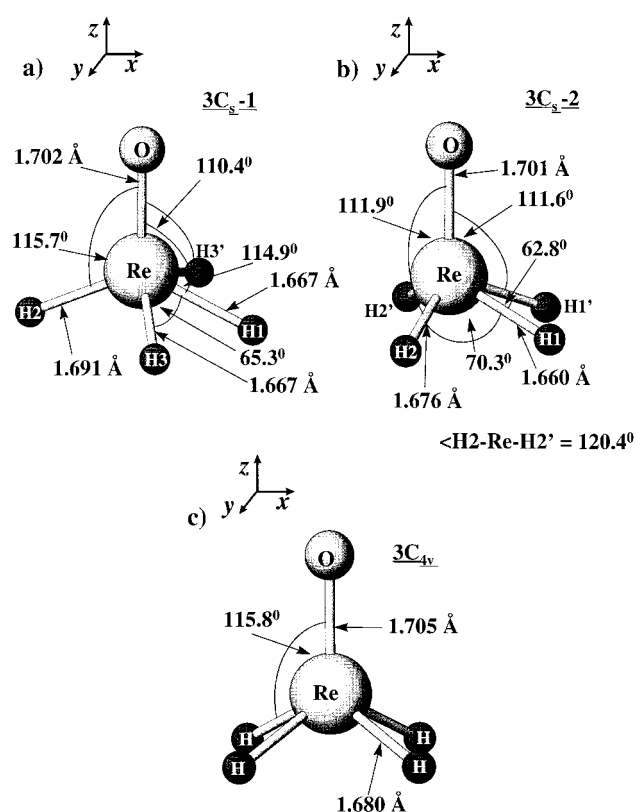

Figure 6. Optimized stationary points for $[ReOH_4]$, with atom labeling and Cartesian coordinate system used for MO analyses. a) **3C$_s$-1** (transition state); b) **3C$_s$-2** (minimum); c) **3C$_{4v}$** (transition state with doubly degenerate imaginary frequency).

anymore, but a transition state connecting the **3C$_s$-2** minima. $[ReOH_4]$ is undoubtedly also fluxional, as evidenced by the relatively low energies of the transition structures **3C$_s$-1** (Table 1), and of the regular square pyramidal structure **3C$_{4v}$**. The latter has one doubly degenerate imaginary vibrational mode like its $[WOH_4]$ and $[WO(CH_3)_4]$ analogues (with a force constant of only -0.122 mDyne Å^{-1} and a frequency of $i445$ cm^{-1}). The molecular dynamics of the rhenium oxohydride are thus expected to be complicated, and somewhat different from the two tungsten species. UCCSD(T) single-point calculations at the DFT optimized structures place **3C$_s$-1** at $+7.8$ kJ mol^{-1} and **3C$_{4v}$** at $+7.5$ kJ mol^{-1} above **3C$_s$-2**. Thus, at higher computational levels, the potential energy surface may even be slightly more shallow, and the existence of the **3C$_s$-1** stationary point appears uncertain.

Structurally, the smaller distortions of **3C$_s$-1** and **3C$_s$-2** (Figure 6a,b) compared with their tungsten analogues (Figure 1a,b) are most clearly seen from the more uniform H-M-O angles and M–H distances. In contrast, the H-M-H angles deviate significantly from a square pyramidal arrangement, as found for $[WOH_4]$. Interestingly, the Re–O distance in $[ReOH_4]$ remains almost constant upon distortion, whereas the W–O distances in $[WOH_4]$ and in $[WO(CH_3)_4]$ contract notably.

B. Bonding: Consider the MO correlation diagram for $[WOH_4]$ in Figure 2 (**1C$_s$-1**, **1C$_s$-2**, **1C$_{4v}$**) and place one additional electron into the LUMO for each structure (3a″

for $3C_s$-1, 5a′ for $3C_s$-2, $1b_2$ for $3C_{4v}$). The detailed analysis of the computed Kohn–Sham MOs for [ReOH$_4$] confirms that this simple one-electron *Aufbau* principle-like picture is a reasonable one. It allows a relatively straightforward understanding of the changes in the structural preferences upon adding one electron to the d^0 system.

In $3C_{4v}$, the nonbonding d_{xy}-type $1b_2$ orbital is now the singly occupied MO (SOMO) of the molecule. Obviously, this situation is electronically much more satisfactory than that in which this MO is left completely empty as in $1C_{4v}$, suggesting a lower tendency for distortion. Moreover, the SOMOs in $3C_s$-1 (3a″) and in $3C_s$-2 (5a′) are both significantly π(Re−O) antibonding (with π_y^* character in $3C_s$-1, but with π_x^* character in $3C_s$-2) and slightly Re−H antibonding (with metal d_{xy} contributions in $3C_s$-1, with $d_{x^2-y^2}$ contributions in $3C_s$-2); this pushes them to relatively high energies. This unfavorable antibonding character of the SOMOs in the distorted structures will also diminish the preference for distortion and will render the regular square pyramidal structure $3C_{4v}$ much more competitive than for the tungsten analogue (cf. Table 1).

The π(Re−O) antibonding character of the SOMOs in $3C_s$-1 and $3C_s$-2 also provides an explanation for the fact that the M−O bond does not contract upon distortion, in contrast to [WOH$_4$] and [WO(CH$_3$)$_4$]. The same holds for the much lower distortions of the H-M-O angles in $3C_s$-1 and $3C_s$-2 compared with $1C_s$-1 and $1C_s$-2 (compare Figure 6 and Figure 1). Natural population analyses for [ReOH$_4$] confirm these considerations (see Table S5 in supporting information).

IV. [ReO(CH$_3$)$_4$]

In view of the above comparison between [WO(CH$_3$)$_4$] and [WOH$_4$], tetramethyloxorhenium (**4**) should be even less inclined to distort than its hydride analogue, which is itself only very slightly distorted (cf. above). This would be consistent with the experimental observation of a regular square pyramidal structure.[22] Indeed, the computations agree with experiment: They show that the square pyramidal structure $4C_{4v}$-1, in which the axial hydrogen atoms are antiperiplanar to the oxo ligand (cf. the analogous structure $2C_{4v}$-1 for [WO(CH$_3$)$_4$] in Figure 3c), is a minimum on the potential energy surface. The vibrational analysis gives a frequency of 207 cm^{-1} and a force constant of +0.080 mDyne Å^{-1} for the E-type mode, which would be the analogue of the imaginary modes of $1C_{4v}$, $2C_{4v}$-1, and $3C_{4v}$. It is thus not even the lowest energy mode of [ReO(CH$_3$)$_4$] (several Re−C rocking modes have lower frequencies and force constants). We have therefore not attempted to locate distorted minima analogous to $2C_s$-1 or $2C_s$-2. Obviously, the combination of one extra d electron *and* methyl instead of hydride ligands is sufficient to prevent distortion.

Incidentally, the more stable antiperiplanar conformation $4C_{4v}$-1 has been correctly posited by Haaland et al. in analyzing the gas electron diffraction data.[22] The synperiplanar structure $4C_{4v}$-2 (see Figure 3e for the analogous structure $2C_{4v}$-2) has four imaginary frequencies and is 44.2 kJ mol^{-1} higher in energy than $4C_{4v}$-1. This is less than the corresponding 58.6 kJ mol^{-1} $2C_{4v}$-1 → $2C_{4v}$-2 energy difference in

[WO(CH$_3$)$_4$] (Table 1), but it still indicates significant hindrance of the rotation around the Re−C single bonds. Thus, while the agostic C−H →M interactions are reduced by adding one electron to the system (e.g., the extra 'agostic' population of the d_{xy} NAO is only 0.078 for $4C_{4v}$-1 compared with 0.241 for $2C_{4v}$-1), they are still surprisingly large (of course, some part of the barriers may be due to repulsions between the methyl hydrogen atoms[15]). One may even speculate whether it is possible to freeze out the individual methyl group rotations in [ReO(CH$_3$)$_4$] at lower temperatures.

The structural data for $4C_{4v}$-1 are in good agreement with the gas electron diffraction results (Table 8).[22] The computed M−C and M−O distances are larger by ca. 0.03 Å, whereas

Table 8. Computed structural parameters for structures $4C_{4v}$-1 and $4C_{4v}$-2 of [ReO(CH$_3$)$_4$], compared with experiment.[a]

	$4C_{4v}$-1	$4C_{4v}$-2	Exptl.[b]
Re−O	1.717	1.717	1.682(3)
Re−C	2.140	2.154	2.117(3)
C−H$_{ax}$	1.107	1.111	av.: 1.113(5)
C−H$_{eq}$	1.106	1.103	
C-Re-O	112.5	109.3	112(1)
C-Re-C (*cis*)	81.5	83.8	82(1)
H$_{ax}$-C-Re	110.3	102.9	av.: 108(1)
H$_{eq}$-C-Re	110.7	115.0	

[a] Distances A−B in Å, angles A-B-C in °. See the analogous atom labeling for $2C_{4v}$-1 and $2C_{4v}$-2 in Figures 3c,e. [b] Gas electron diffraction results, see ref. [22]. A conformation as in $4C_{4v}$-1 was assumed in the refinement.

the bond angles agree very well. Only averaged C−H distances and H-C-Re angles were given by Haaland et al., assuming C_{3v} local symmetry of the methyl groups.[22] It turns out that, in spite of the agostic interactions and of the appreciable rotational barrier, this assumption is also well-founded: the methyl groups in $4C_{4v}$-1 deviate only little from local threefold symmetry (in contrast to $4C_{4v}$-2). Early qualitative MO considerations have been used by Gibson et al.[21c] to interpret the ESR spectrum of [ReO(CH$_3$)$_4$]. The Kohn–Sham MOs computed here are consistent with the resulting simple one-electron picture (Figure 2). Thus, the SOMO is a metal d_{xy}-type nonbonding b_2 MO, with some coefficients at hydrogen due to agostic interactions (cf. above).

Conclusions

Our quantum chemical calculations indicate novel types of fluxional structures for several of the five-coordinate d^0 and d^1 MOR$_4$ title compounds. These results extend the already impressive range of unusual structures for d^0 complexes (see Introduction). The peculiar structural behavior results from a competition between π-bonding to the oxo ligand and σ-bonding to the other four ligands. The C_s-1 structure type found to be the most stable for the d^0 systems [WOH$_4$] (**1**) and [WO(CH$_3$)$_4$] (**2**) may be related to a structure type of [MX$_2$R$_3$] complexes denoted edge-bridged tetrahedral by Ward et al. in

an independent, parallel computational study (also see Section I).[25] For the present [MXR$_4$] complexes, a second, to our knowledge unprecedented type of distorted square pyramidal structure, **C$_s$-2** (cf. Figures 1b, 3b, and 6b), was found to be important. It is the lowest energy minimum for the d^1 complex [ReOH$_4$] (**3**) and is also very competitive for the d^0 systems **1** and **2**. Matters for the methyl compounds **2** and **4** are further complicated by agostic interactions. These may lead to surprisingly large conformational energy differences, which depend additionally on the skeletal distortions.

We have provided detailed structural and spectroscopic predictions, in particular for [WO(CH$_3$)$_4$] (**2**), as we hope that the unusual properties predicted for this interesting compound may be accessible to experimental confirmation. In spite of the coordinatively unsaturated character, tetramethyloxotungsten and related tetraalkyl systems are not unlikely synthetic targets. Probably the most closely related, somewhat more complicated experimental example is the structure of [WONp$_3$(NEt$_2$)] (Np = neopentyl) (**5**).[50] Consider the three methyl groups 1, 3 and 3′ in **2C$_s$-1** (Figure 3a) replaced by neopentyl ligands and methyl group 2 by the diethylamido group. The angles between the ligands for the two systems correspond closely. Notably, the amido ligand in **5** is oriented parallel to the W−O bond. This is the optimum orientation for π-donation from the amido ligand to the metal (cf. the 3a″ LUMO for **1C$_s$-1** in Figure 2). As other, more remote structural examples, one might consider [ReO$_2$Np$_3$] (the bonding situation is more complex and apparently involves H-bonding interactions)[51] or [MoO{OC(CF$_3$)$_3$}$_4$] (the quality of the structural data is insufficient to allow detailed conclusions).[52] In each case, a competition between σ- and π-bonding is important (see also the discussion in ref. [25]).

Our previous calculations on hexamethyl systems have shown that structural distortions are more pronounced in the 4d series than in the 5d series (e.g., [Mo(CH$_3$)$_6$] is somewhat more distorted than [W(CH$_3$)$_6$]), as relativistic effects increase the ligand–ligand repulsions for the heavier metals.[12] We thus expect the molybdenum analogues [MoOR$_4$] of the tungsten complexes studied here to be even more significantly distorted.[53a] Other d^0 systems with one π-donor ligand plus four purely σ-donating ligands should be expected to exhibit similar distortions as those found here. Indeed, stronger π-donors like nitride or alkynyl ligands should favor more strongly distorted (and more rigid?) structures. This is confirmed by our preliminary calculations on the d^0 alkynyl model complex [Re(CH)H$_4$], which is computed to have a strongly distorted structure of the C$_s$-2 type, with a considerably steeper potential energy surface than [WOH$_4$] (**1**).[53b] In contrast, [NbClH$_4$] and [TaClH$_4$] are cases with a weaker apical π-donor and thus are less distorted than **1**.

The range of compounds, where such nonclassical low-symmetry d^0 (and d^1) structures may be expected, is probably much larger than previously assumed. Fluxional structures are in general quite common for five-coordination. However, our ongoing investigations on heteroleptic methyl/halogeno complexes of tungsten, [WX$_n$(CH$_3$)$_{6-n}$] (X = F, Cl; $n = 0-6$),

indicate that many of these six-coordinate systems feature also unusual distorted structures.[54] Thus, there should be an entire area of d^0 complexes with interesting structures worth investigating.

[1] Examples for computational work: a) L. Seijo, Z. Barandiaran, S. Huzinaga, *J. Chem. Phys.* **1991**, *94*, 762; b) M. Kaupp, P. von R. Schleyer, H. Stoll, H. Preuss, *J. Chem. Phys.* **1991**, *94*, 1360; c) M. Kaupp, P. von R. Schleyer, H. Stoll, H. Preuss, *J. Am. Chem. Soc.* **1991**, *113*, 6012; d) M. Kaupp, P. von R. Schleyer, *J. Am. Chem. Soc.* **1992**, *114*, 491; e) M. Kaupp, P. von R. Schleyer, H. Stoll, M. Dolg, *J. Am. Chem. Soc.* **1992**, *114*, 8202; f) M. Kaupp, O. P. Charkin, P. von R. Schleyer, *Organometallics* **1992**, *11*, 2767; g) I. Bytheway, R. J. Gillespie, T.-H. Tang, R. F. W. Bader, *Inorg. Chem.* **1995**, *34*, 2407.

[2] The earliest experimental indications for bent gas-phase structures of some alkaline-earth dihalides date back to the electric quadrupole deflection experiments of Klemperer et al.; see, e.g.: L. Wharton, R. A. Berg, W. Klemperer, *J. Chem. Phys.* **1963**, *39*, 2023, and references therein.

[3] Recent structure determinations of dialkyl compounds: a) C. Eaborn, P. B. Hitchcock, K. Izod, J. D. Smith, *J. Am. Chem. Soc.* **1994**, *116*, 12071. b) C. Eaborn, P. B. Hitchcock, K. Izod, Z.-R. Lu, J. D. Smith, *Organometallics* **1996**, *15*, 4783; c) C. Eaborn, S. A. Hawkes, P. B. Hitchcock, J. D. Smith, *J. Chem. Soc. Chem. Commun.* **1997**, 1961.

[4] a) Metallocenes: J. S. Ghotra, M. B. Hursthouse, A. J. Welch, *J. Chem. Soc. Chem. Commun.* **1973**, 669; b) R. A. Andersen, D. H. Templeton, A. Zalkin, *Inorg. Chem.* **1978**, *17*, 2317.

[5] See, e.g.: a) C. A. Jolly, D. S. Marynick, *Inorg. Chem.* **1989**, *28*, 2893; b) M. Kaupp, P. von R. Schleyer, *J. Phys. Chem.* **1992**, *96*, 7316; c) C. W. Bauschlicher, Jr., M. Sodupe, H. Partridge, *J. Chem. Phys.* **1992**, *96*, 4453; d) E. D. Glendening, D. Feller, *J. Phys. Chem.* **1996**, *100*, 4790; e) P. E. M. Siegbahn, *J. Phys. Chem.* **1993**, *97*, 9096.

[6] P. M. Morse, G. S. Girolami, *J. Am. Chem. Soc.* **1989**, *111*, 4114.

[7] S. K. Kang, H. Tang, T. A. Albright, *J. Am. Chem. Soc.* **1993**, *115*, 1971.

[8] A. Haaland, A. Hammel, K. Rypdal, H. V. Volden, *J. Am. Chem. Soc.* **1990**, *112*, 4547.

[9] M. Kaupp, *J. Am. Chem. Soc.* **1996**, *118*, 3018.

[10] V. Pfennig, K. Seppelt, *Science* **1996**, *271*, 626.

[11] See also, e. g.: a) S. K. Kang, T. A. Albright, P. Eisenstein, *Inorg. Chem.* **1989**, *28*, 1611; b) M. Shen, H. F. Schaeffer, III, H. Partridge, *J. Chem. Phys.* **1993**, *98*, 508; c) V. Jonas, G. Frenking, J. Gauss, *Chem. Phys. Lett.* **1992**, *194*, 109; d) D. G. Musaev, O. P. Charkin, *Sov. J. Coord. Chem.* **1989**, *15*, 102; e) A. Zyubin, D. G. Musaev, O. P. Charkin, *Russ. J. Inorg. Chem.* **1992**, *37*, 1214; f) C. R. Landis, T. Cleveland, T. K. Firman, *J. Am. Chem. Soc.* **1995**, *117*, 1859; g) P. E. M. Siegbahn, M. R. A. Blomberg, *J. Am. Chem. Soc.* **1993**, *115*, 4191.

[12] M. Kaupp, *Chem. Eur. J.* **1998**, *4*, 1678–1686.

[13] R. Hoffmann, J. M. Howell, E. L. Muetterties, *J. Am. Chem. Soc.* **1972**, *94*, 3047.

[14] A. R. Rossi, R. Hoffmann, *Inorg. Chem.* **1975**, *14*, 365.

[15] T. A. Albright, J. K. Burdett, M.-H. Whangbo, *Orbital Interactions in Chemistry*, Wiley, New York, **1985**.

[16] C. Pulham, A. Haaland, A. Hammel, K. Rypdal, H. P. Verne, H. V. Volden, *Angew. Chem.* **1992**, *104*, 1534; *Angew. Chem. Int. Ed. Engl.* **1992**, *31*, 1464.

[17] C. J. Piersol, R. D. Profilet, P. Fanwick, I. P. Rothwell, *Polyhedron* **1993**, *12*, 1779.

[18] T. A. Albright, H. Tang, *Angew. Chemie* **1992**, *104*, 1532; *Angew. Chem. Int. Ed. Engl.* **1992**, *31*, 1462.

[19] See, e.g.: W. A. Nugent, J. M. Mayer, *Metal–Ligand Multiple Bonds*, Wiley, New York, **1988**, and references therein.

[20] K. Seppelt, unpublished results, personal communication.

[21] a) K. Mertis, J. F. Gibson, G. Wilkinson, *J. Chem. Soc. Chem. Commun.* **1974**, 93; b) K. Mertis, D. H. Williamson, G. Wilkinson, *J. Chem. Soc. Dalton Trans.* **1975**, 607; c) J. F. Gibson, K. Mertis, G. Wilkinson, *J. Chem. Soc. Dalton Trans.* **1975**, 1093.

[22] A. Haaland, H. P. Verne, H. V. Volden, W. A. Herrmann, P. Kiprof, *J. Mol. Struct.* **1995**, *352/353*, 153.

[23] M. A. Pietsch, M. Couty, M. B. Hall, *J. Phys. Chem.* **1995**, *99*, 16325.

[24] R. H. Cayton, M. H. Chisholm, E. R. Davidson, *Inorg. Chem.* **1991**, *30*, 1020.

[25] T. R. Ward, H.-B. Bürgi, F. Gilardoni, J. Weber, *J. Am. Chem. Soc.* **1997**, *119*, 11974.

[26] A. D. Becke, *Phys. Rev. A* **1988**, *38*, 3098.

[27] J. P. Perdew, *Phys. Rev. B* **1986**, *33*, 8822.

[28] M. Dolg, U. Wedig, H. Stoll, H. Preuss, *J. Chem. Phys.* **1987**, *86*, 866; D. Andrae, U. Häussermann, M. Dolg, H. Stoll, H. Preuss, *Theor. Chim. Acta* **1990**, *77*, 123.

[29] A. Bergner, M. Dolg, W. Küchle, H. Stoll, H. Preuss, *Mol. Phys.* **1993**, *80*, 1431.

[30] T. H. Dunning, H. Hay, in *Methods of Electronic Structure Theory; Modern Theoretical Chemistry, Vol. 3* (Ed.: H. F. Schaefer, III), Plenum, New York, **1977**.

[31] a) C. van Wüllen, *Int. J. Quant. Chem.* **1996**, *58*, 147; b) T. V. Russo, R. L. Martin, P. J. Hay, *J. Phys. Chem.* **1995**, *99*, 17085; c) further examples in the context of NMR chemical shift calculations are: M. Kaupp, V. G. Malkin, O. L. Malkina, D. R. Salahub, *Chem. Phys. Lett.* **1995**, *235*, 382; M. Kaupp, V. G. Malkin, O. L. Malkina, D. R. Salahub, *Chem. Eur. J.* **1996**, *2*, 24; M. Kaupp, *Chem. Eur. J.* **1996**, *2*, 348.

[32] deMon program: D. R. Salahub, R. Fournier, P. Mlynarski, I. Papai, A. St-Amant, J. Ushio, in *Density Functional Methods in Chemistry* (Eds.: J. Labanowski, J. Andzelm), Springer, New York, **1991**; A. St-Amant, D. R. Salahub, *Chem. Phys. Lett.* **1990**, *169*, 387.

[33] a) Gaussian 92/DFT, Revision G, M. J. Frisch, G. W. Trucks, M. Head-Gordon, P. M. W. Gill, M. W. Wong, J. B. Foresman, B. G. Johnson, H. B. Schlegel, M. A. Robb, E. S. Replogle, R. Gomperts, J. L. Andres, K. Raghavachari, J. S. Binkley, C. Gonzalez, R. L. Martin, D. I. Fox, D. J. DeFrees, J. Baker, J. P. Stewart, J. A. Pople, Gaussian, Pittsburgh, **1992**; b) Gaussian 94, Revisions B2, G.2, M. J. Frisch, G. W. Trucks, H. B. Schlegel, P. M. W. Gill, B. G. Johnson, M. A. Robb, J. R. Cheeseman, T. Keith, G. A. Petersson, J. A. Montgomery, K. Raghavachari, M. A. Al-Laham, V. G. Zakrzewski, J. V. Ortiz, J. B. Foresman, C. Y. Peng, P. Y. Ayala, W. Chen, M. W. Wong, J. L. Andres, E. S. Replogle, R. Gomperts, R. L. Martin, D. J. Fox, J. S. Binkley, D. J. Defrees, J. Baker, J. P. Stewart, M. Head-Gordon, C. Gonzalez, J. A. Pople, Gaussian, Pittsburgh, **1995**.

[34] C. Peng, H. B. Schlegel, *Isr. J. Chem.* **1993**, *33*, 449; C. Peng, P. Y. Ayala, H. B. Schlegel, M. J. Frisch, *J. Comp. Chem.* **1995**, *16*, 49.

[35] a) A. E. Reed, F. Weinhold, *J. Chem. Phys.* **1985**, *83*, 1736; b) A. E. Reed, L. A. Curtiss, F. Weinhold, *Chem. Rev.* **1988**, *88*, 899.

[36] MOLPRO is a package of ab initio programs written by H.-J. Werner and P. J. Knowles, with contributions from J. Almlöf, R. D. Amos, A. Berning, M. J. O. Deegan, F. Eckert, S. T. Elbert, C. Hampel, R. Lindh, W. Meyer, A. Nicklass, K. Peterson, R. Pitzer, A. J. Stone, P. R. Taylor, M. E. Mura, P. Pulay, M. Schütz, H. Stoll, T. Thorsteinsson, D. L. Cooper. For the coupled-cluster treatments, cf: a) C. Hampel, K. Peterson, H.-J. Werner, *Chem. Phys. Lett.* **1992**, *190*, 1; b) P. J. Knowles, C. Hampel, H.-J. Werner, *J. Chem. Phys.* **1993**, *99*, 5219 [UCCSD(T)].

[37] A. W. Ehlers, M. Böhme, S. Dapprich, A. Gobbi, A. Höllwarth, V. Jonas, K. F. Köhler, R. Stegmann, A. Veldkamp, G. Frenking, *Chem. Phys. Lett.* **1993**, *208*, 111.

[38] V. G. Malkin, O. L. Malkina, M. E. Casida, D. R. Salahub, *J. Am. Chem. Soc.* **1994**, *116*, 5898.

[39] V. G. Malkin, O. L. Malkina, L. A. Eriksson, D. R. Salahub, in *Modern Density Functional Theory: A Tool for Chemistry; Theoretical and Computational Chemistry, Vol. 2* (Eds.: J. M. Seminario, P. Politzer), Elsevier, Amsterdam, **1995**.

[40] W. Kutzelnigg, U. Fleischer, M. Schindler, in *NMR—Basic Principles and Progress, Vol. 23*, Springer, Heidelberg, **1990**, pp. 165 ff.

[41] J. P. Perdew, Y. Wang, *Phys. Rev. B* **1992**, *45*, 13244; J. P. Perdew in *Electronic Structure of Solids* (Eds.: P. Ziesche, H. Eischrig), Akademie, Berlin, **1991**, J. P. Perdew, J. A. Chevary, S. H. Vosko, K. A. Jackson, M. R. Pederson, D. J. Singh, C. Fiolhais, *Phys. Rev. B* **1992**, *46*, 6671.

[42] See, e.g.: W. McFarlane, H. C. E. McFarlane, in *Multinuclear NMR* (Ed.: J. Mason), Plenum, New York, **1987**, pp. 403 ff.

[43] For the original introduction of the term agostic interaction, see M. Brookhart, M. L. H. Green, *J. Organomet. Chem.* **1983**, *250*, 395. We employ the term to indicate significant hyperconjugative interactions between C−H bonds and empty metal orbitals, without requiring a situation close to the breaking of the C−H bond.

[44] Individual rotation of methyl groups 1 and 2 into the synperiplanar orientation costs only ca. 1.6 kJ mol^{-1} and 0.5 kJ mol^{-1}, respectively.

[45] In such cases, the H_{eq}-C-H_{eq} angles are several degrees larger than 109.5°, whereas the H_{eq}-C-H_{ax} angles are smaller. In organic chemistry, this type of compensation is sometimes referred to as a Thorpe–Ingold effect (see, e.g.: R. Boese, D. Bläser, N. Niederprüm, M. Nüsse, W. A. Brett, P. von R. Schleyer, M. Bühl, N. J. R. van Eikema Hommes, *Angew. Chem.* **1992**, *31*, 314; *Angew. Chem. Int. Ed. Engl.* **1992**, *104*, 356, and references therein).

[46] In the case of extremely low energy barriers, dynamic effects may appreciably alter IR spectra at higher temperatures (see e.g.: M. Bühl, W. Thiel, *Inorg. Chem.* **1997**, *36*, 2922).

[47] See, e.g.: M. Kaupp, O. L. Malkina, V. G. Malkin, *J. Chem. Phys.* **1997**, *106*, 9201, and references therein.

[48] See, e.g.: W. A. Herrmann, F. E. Kühn, P. W. Roesky, *J. Organomet. Chem.* **1995**, *485*, 243.

[49] Further refinement of the X-ray data interpreted previously as a distorted prism[10] does now confirm our computational prediction of a regular structure[9, 12] (K. Seppelt et al., *Chem. Eur. J.* **1998**, *4*, 1687–1691.

[50] J. P. Le Ny, M.-T. Youinou, J. A. Osborn, *Organometallics* **1992**, *11*, 2413.

[51] S. Cai, D. M. Hoffmann, D. A. Wierda, *J. Chem. Soc. Chem. Commun.* **1988**, 313.

[52] D. A. Johnson, J. C. Taylor, A. B. Waugh, *J. Inorg. Nucl. Chem.* **1980**, *42*, 1271.

[53] a) This is supported by preliminary DFT results (at the same computational level as used here), which indicate the regular square pyramid to be above the distorted C_s structures by ca. 120 kJ mol^{-1} for [MoOH$_4$], and by ca. 25 kJ mol^{-1} for [MoO(CH$_3$)$_4$] (M. Kaupp, unpublished results). This suggests that the molybdenum systems might be less fluxional than their tungsten analogues; b) DFT energies indicate that for Re(CH)H$_4$, the C_{4v} structure (degenerate transition state) is ca. 227 kJ mol^{-1} above the **C$_s$-2** minimum, and the **C$_s$-1** transition state is also less stable by ca. 14 kJ mol^{-1}.

[54] M. Kaupp, unpublished results.